Hydrogen-accelerated white etching area formation in bearings under rolling contact fatigue

X.Z. Liang[1], P.E.J. Rivera-Díaz-del-Castillo [*]

Department of Engineering, Lancaster University, Lancaster LA1 4YW, UK

ARTICLE INFO

ABSTRACT

The presence of hydrogen can dramatically facilitate microstructural alterations in components subjected to rolling contact fatigue (RCF) potentially leading to premature failure. A dislocation-assisted carbon migration model is developed to describe the formation of hydrogen-influenced microstructural alterations such as white etching areas; the model incorporates rolling parameters such as maximum contact stress, number of cycles, rotational speed, and temperature. Kinetic Monte Carlo is adopted to describe hydrogen-dislocation interactions which alters dislocation mobility, accelerating white etching area formation whilst reducing fatigue life. The results are experimentally validated by microstructural characterisation and RCF testing.

1. Introduction

Bearings contain high-strength wear-resistant elements subjected to rolling contact fatigue (RCF) [1–5]. During service, such elements often encounter extreme conditions such as high contact stress, long-term fatigue cycles, fast rotational speed and elevated temperature [1,6]. As a result, they often fail by cracking or spalling; such failure is significantly accelerated in the presence of hydrogen, which is present in a large number of environmental conditions [6]. Therefore, it is of significant importance to understand the microstructural transitions leading to RCF failure, especially in the presence of hydrogen.

RCF can lead to surface and subsurface cracking. The surface cracking can essentially be avoided by proper lubrication minimising solid-to-solid contact. Subsurface cracking is manifested by microstructural alterations, such as the formation of white etching areas (WEAs), dark etching regions (DERs) and white etching bands (WEBs) [1,4,7–9]. The changes in microstructure influence bearing properties leading to failure.

WEAs are usually the first form of microstructural change under RCF [4,10]; they typically occur around $0.001L_{10}$ [4]. L_{10} is the number of rotations at which 10% of bearings fail [4]. It has been reported that WEAs are ferritic structures composed of dislocation cells of 10 to 100 nm in size, sometimes referred to as butterflies because of their wing shape [4,8,10] that spread roughly 45° to the over-rolling direction. WEAs often occur adjacent to non-metallic inclusions and primary carbides [4,10,11]; they form due to carbon migration from dislocation atmospheres to cell boundaries, leading to extreme grain refinement. DERs tend to occur at around $0.1L_{10}$ and grow with an increase in stress cycles [3]; they are driven by the subsurface shear stress component and are accompanied by a dislocation-driven redistribution of carbon from the matrix to temper carbides [12]. WEBs form roughly at $0.1L_{50}$ [2]. They are decorated by lenticular carbides (LCs) formed at 30° and 70° to the over-rolling direction when viewed in the circumferential section, which is the plane perpendicular to the main axis of the rod. LCs result from carbon previously at the matrix. Recently, Fu et al. [2–4] have proposed a dislocation-assisted carbon migration theory to model such microstructural alterations in bearings. The theory assumes that gliding dislocations redistribute carbon forming WEAs, DERs and WEBs. By applying this theory, the aforementioned microstructural alternations have been well described in 100Cr6 bearings, hence the RCF failure can be predicted [2–4].

Hydrogen ingress in bearings may occur for a variety of reasons, for example, exposure to corrosive environments and oil decomposition [14]. It is well accepted that material properties can be greatly degraded by hydrogen [15,16]. In the case of bearing elements, hydrogen can lead to an early failure during RCF [6,14,17–21]. Experimental results demonstrate that microstructural alterations are facilitated by hydrogen, signalling hydrogen-induced premature RCF failure [6,20]. A few studies have attempted to describe the factors affecting hydrogen behaviour in bearings [22–24], nevertheless there is no unified model available to quantitatively describe such hydrogen-facilitated microstructural alterations. The present work introduces a correction factor to the dislocation-assisted carbon migration theory to describe

---
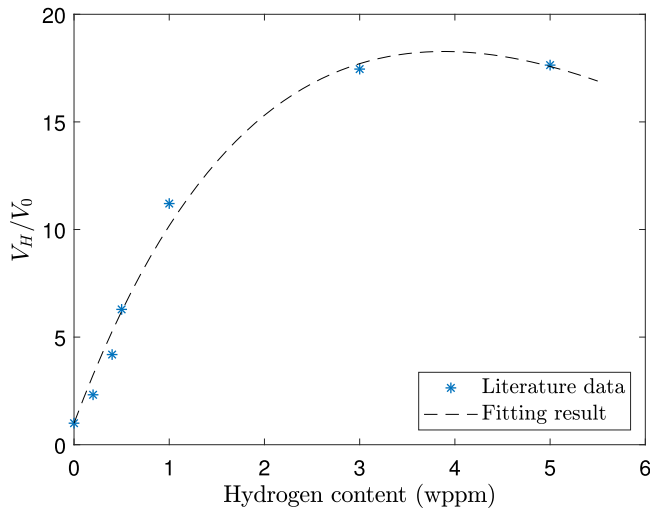
Fig. 1. Hydrogen influence on dislocation mobility; literature data extracted from Ref. [13].

microstructure evolution during RCF. The correction factor is taken from density functional theory and kinetic Monte Carlo (kMC) calculations on dislocation-hydrogen interactions. The new model describes the experimental results performed in this work, as well as the majority of the reports in the literature. The need to extend the model to low and high contact pressures is pointed out.

2. Theory

2.1. Dislocation-assisted carbon migration

The work by Fu and Rivera-Díaz-del-Castillo [4] is firstly reviewed. Under RCF, the subsurface strain is realised by dislocation glide during which an amount of carbon atoms n_c is captured around the dislocation line forming an atmosphere:

$$n_c = 3 \left(\frac{\pi}{2}\right)^{\frac{1}{3}} \left(\frac{A D t_C}{kT}\right)^{\frac{2}{3}} C_V^i, \tag{1}$$

where A denotes the interaction energy between a carbon atom and the dislocation strain field, D is the diffusion coefficient of carbon atoms in iron, $t_C = \frac{1}{\dot{N}}$, here the $\dot{N}$ denotes the frequency of RCF stress cycles per unit time, k is the Boltzmann constant, T represents temperature, and C_V^i is the carbon concentration in matrix. Assuming the number of carbon atoms n_c captured per unit length of dislocation is known, the carbon flux resulting from dislocation glide can be expressed as:

$$J_d = \rho_m \Delta L \dot{N} n_c, \tag{2}$$

where ρ_m is the density of mobile dislocations; ΔL represents the average glide distance of mobile dislocations. Here, the product of $\rho_m \Delta L$ is related to the plastic strain per stress cycle

$$\Delta \gamma = b \rho_m \Delta L, \tag{3}$$

where b is the magnitude of the Burgers vector. Combining Eqs. (1)–(3), the carbon flux can be expressed by

$$J_d = \frac{\Delta \gamma \dot{N}}{b} \left[3 \left(\frac{\pi}{2}\right)^{\frac{1}{3}} \left(\frac{A D t_C}{kT}\right)^{\frac{2}{3}} C_V^i \right]. \tag{4}$$

This equation can be used to evaluate the carbon flux in bearings under RCF. It has been shown that the evolution of WEAs, DERs and WEBs can be modelled by it [2–4].

2.2. Hydrogen-altered dislocation mobility

It has been extensively reported that the mobility of dislocations can be greatly affected by hydrogen [13,25,26]. In recent years, the development of electronic and atomistic simulations has significantly enhanced the understanding of hydrogen-dislocation interactions. Katzarov et al. [13] have performed density functional theory informed simulations of dislocation-hydrogen interactions. Through kMC modelling, they showed that dislocation mobility can be greatly affected depending on hydrogen concentration. The results by Katzarov et al. [13] are shown in Fig. 1; where V_H and V_0 are the dislocation velocity in the presence and absence of hydrogen, respectively. V_H/V_0 thus indicates the hydrogen influence on dislocation mobility:

$$\frac{V_H}{V_0} = 1 + B_1 C_H + B_2 \left[\exp(-B_3 C_H) - 1\right], \tag{5}$$

with fitting parameters of $B_1 = -3.273$, $B_2 = -38.31$ and $B_3 = 0.22$.

2.3. Hydrogen-facilitated white etching area formation

Inserting Eq. (5) into Eq. (4), a correction to carbon flux due to hydrogen can be expressed as

$$J_d = \frac{\Delta \gamma \dot{N}}{b} \frac{V_H}{V_0} \left[3 \left(\frac{\pi}{2}\right)^{\frac{1}{3}} \left(\frac{A D t_C}{kT}\right)^{\frac{2}{3}} C_V^i \right]. \tag{6}$$

WEAs appear when dislocation cells form, transporting carbon to their cell boundaries as demonstrated by atom probe tomography [27]. Fig. 2 shows a schematic diagram of cell formation in WEAs. The critical argument in this work is that the flux of carbon towards the cell boundaries is accelerated by hydrogen, and this is described by Eq. (6). If we assume the cell radius to be r_c and the cell wall thickness to be h_c, thus carbon mass conservation is held when

$$\frac{4}{3}\pi r_c^3 C_V^0 = \frac{4}{3}\pi(r_c - h_c)^3 C_V^i + \frac{4}{3}\pi \left[r_c^3 - (r_c - h_c)^3\right] C_V^w, \tag{7}$$

where C_V^0 is the total carbon concentration per unit volume in the system which is calculated by $C_V^0 = \frac{2 C_0}{a_m^3}$, where a_m denotes the lattice parameter of ferrite which equals to $\frac{2b}{\sqrt{3}}$; C_V^w is the carbon concentration in the cell wall which is calculated by $\frac{2 C_w}{a_m^3}$. The parameter Cell% = $\left(1 - C_v^i/C_v^0\right) \times 100\%$ [4] can be used to indicate the progress in WEAs formation, and a value of Cell% = 99.9% can characterise the completion in the formation of WEAs [4].

3. Validation

3.1. Experimental

To validate the proposed model, a set of experiments was conducted. Bearing grade 100Cr6 (SAE 52100) was investigated in this study. Table 1 lists its chemical composition as measured by optical emission spectroscopy. The specimens were first quenched from an austenitisation temperature of 840 °C to room temperature and tempered at 160 °C for 90 min. Rod samples of 9.53 mm diameter were prepared for rolling contact fatigue tests. Surface roughness of 0.12 μm was measured for the tested rod specimens.

Hydrogen charging was electrochemically performed in a 3.5 wt% NaCl solution at 80 °C; its duration was 5 days at a current density of 10 mA/cm². Lacomit varnish was painted to cover the remaining part of the sample to reduce corrosion. Ethanol was used immediately after charging to clean the sample, and Lacomit remover was used to remove the paint. It has been shown that under such conditions 100Cr6 will be saturated with ~5 ppm hydrogen [19,20]. The hydrogen charging applied in this study can introduce sufficient hydrogen to saturate the material.
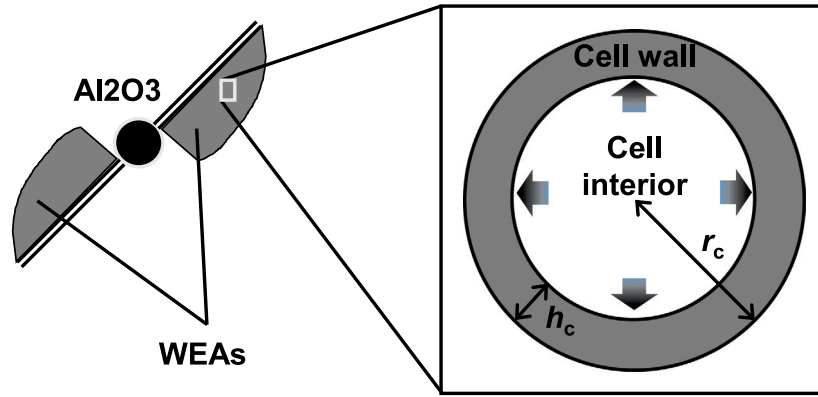
Fig. 2. Schematic diagram showing cell formation in WEAs.

Table 1
Chemical composition of the investigated steels.

Element	C (wt.%)	Cr (wt.%)	Ni (wt.%)	Mn (wt.%)	Si (wt.%)	Mo (wt.%)	Cu (wt.%)	P (ppm)	S (ppm)
	0.95	1.50	0.02	0.01	0.27	0.01	0.02	130	20
Al (ppm)	Ti (ppm)	Ca (ppm)	Pb (ppm)	Sn (ppm)	As (ppm)	Sb (ppm)	Bi (ppm)	N (ppm)	O (ppm)
247	6	2	16	10	20	10	30	20.3	6.1

Table 2
RCF samples tested in this study.

P_0 (GPa)	RCF cycles until failure ($\times 10^6$)		
	Hydrogen-lean	Hydrogen-charged	
3.9	39.9	21.4	31.4
4.5	36.8	12.9	34.2
5.0	28.2	7.9	16.3

Rolling contact fatigue testing was performed on a three ball-on-rod fatigue tester. The setup details can be found in Ref. [4]. In this study, maximum contact pressures (P_0) of 3.9, 4.5 and 5.0 GPa were applied at a rotational speed of 3600 rpm, which equals $\dot{N} = 9000$ cpm (cycles per minute) for this geometry. A vibration sensor was attached to the head of test rig to detect spalling by monitoring an abnormal increase in vibration levels. The tests performed in this study were stopped automatically by the rig once spalling was present on the rod specimen. Table 2 shows the test results. The fatigue lives of hydrogen-lean samples are between 2.82×10^7 and 3.99×10^7 cycles at different applied stresses, while the fatigue lives of hydrogen-charged samples are reduced systematically being between 0.79×10^7 and 3.42×10^7 cycles.

To investigate the subsurface microstructure, samples were prepared to show the circumferential section. Fig. 3 shows typical WEAs formed in hydrogen-charged specimens under 3.9 GPa contact stress with 21.4×10^6 RCF cycles. In contrast, no WEAs was found in hydrogen-lean samples. The size of these WEAs ranges from 10 to 30 μm, which is comparable with other reported sizes in both hydrogen-lean [1,4,28] and hydrogen-charged [6,10] bearings.

As the formation rate of WEAs is dictated by carbon redistribution [4], the occurrence of such hydrogen-accelerated WEAs implies a faster carbon redistribution process in hydrogen-charged specimens. Evans et al. [10] reported that the cell size in WEAs in hydrogen-rich bearing elements is about 10 to 60 nm. In this paper, the radius of the cells is assumed to be 25 nm to model the hydrogen-assisted WEA formation. The strain accumulation under RCF is taken from [4]

$$\Delta\gamma_0 = 0.0003 \times \left(\frac{\tau_e}{\tau_Y} - 1\right)^3, \tag{8}$$

where τ_e and τ_Y are the applied shear stress and shear yield strength, respectively. In RCF, the applied shear stress is calculated by $\tau_e = $
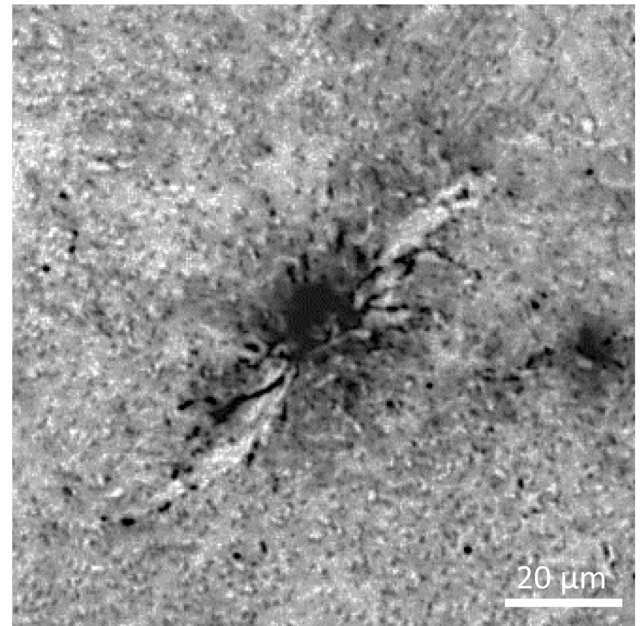
Fig. 3. A typical WEA in hydrogen-charged RCF specimens under optical microscope; test condition $P_0 = 3.9$ GPa with 21.4×10^6 RCF cycles.

$\sqrt{\left(\frac{p_c}{2}\right)^2 + q_c^2}$. The stress p_c applied normal to the crack face is associated with the stress components σ_{iy} and σ_{iz}: $p_c = -\sin\frac{\pi}{4}\left(\sigma_{iy} + \sigma_{iz}\right)$. The friction stress on the rubbing crack face $q_c = \mu p_c$, where μ is the friction coefficient. The shear strength can be estimated from the tensile yield strength by $\tau_Y = \sigma_Y/\sqrt{3}$. It should be noted that work hardening is dependent upon the applied stress [29]. For contact stress over 3.0 GPa, the equation $\sigma_Y = -90.7 + 2.876 H_V$ is used to estimate the yield strength [30]. For contact stresses lower than 3.0 GPa the value $\sigma_Y = 1.28$ GPa is used; this has been shown to be is suitable to model microstructural alternations at moderate contact stress [4]. Table 3 lists the input parameters in this study.
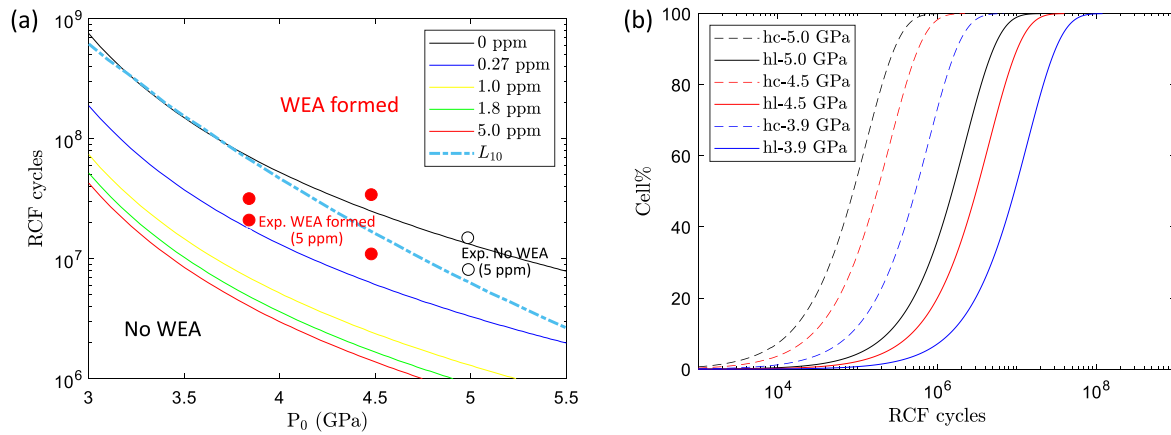
Fig. 4. Modelling of WEA formation for $\dot{N}$ = 9000 cpm and T = 30 °C. (a) RCF cycles to form WEAs for various hydrogen contents (from 0 to 5 ppm) as well as L_{10} fatigue life plot, experimental results at 3.9 GPa, 4.5 GPa and 5.0 GPa are also marked in the figure; (b) Cell% in hydrogen-lean (hl) and hydrogen-charged (hc) specimens.

Table 3
Input parameters in this study.

Parameter	Value	Ref.
b	0.248 nm	[31]
A	3×10^{-30} Nm^2	[32]
C_0	3.1 at.%	[33]
C_w	7.0 at.%	[4]
D_0	6.2×10^{-7} m^{2}s^{-1}	[4]
E	80 kJ mol^{-1}	[34]
r_c	25 nm	This study
$H_{V,1kgf}$	780	This study
T	30 °C	This study
μ	0.3	[4]

Fig. 4(a) shows the full formation of WEAs with different levels of hydrogen content under test condition $\dot{N}$ = 9000 cpm at T = 30 °C as well as a L_{10} fatigue life plot. Here, the L_{10} plot is for referencing the presence of failure at different stresses. Its value is calculated by equation $L_{10} = a \left(\frac{C}{P_L} \right)^{p_{10}}$, where a is a constant that takes materials properties into account [1]; C is the basic dynamic loading rating, and a value of 1147.5 is used in this study; P_L denotes the equivalent dynamic bearing load; p_{10} is the exponent for the life equation which equals to 3 for ball bearings [1]. The calculation of C and P_L is based on ISO 281, while the factor a is estimated to be 2 for the materials used in this study [1]. L_{10} represents the conditions under which 10% of bearings fail, incorporating widespread statistical data to support it. The model results show that, in hydrogen-rich samples, WEAs appear more than an order of magnitude earlier in RCF cycles; this holds for a wide range of contact stress. The experimental results are also added in the figure. The model describes well WEA formation under 3.9 and 4.5 GPa but failed in the prediction of 5.0 GPa. This is due to excessive microplasticity with the high applied stress, which will be discussed in Section 4.2. Fig. 4(b) shows the typical WEA formation progress under maximum contact stresses of 3.9, 4.5 and 5.0 GPa in hydrogen-lean to hydrogen-rich conditions. The model result suggests that WEAs could occur within 10^8 RCF cycles in hydrogen-lean samples under 3.9 GPa, whilst it is 4×10^6 RCF cycles in hydrogen-charged samples. The experimental observations shown in Table 2 indicate that, under 3.9 GPa contact stress, WEAs are present in hydrogen-charged samples with 21.4×10^6 RCF cycles (5 ppm). This is in agreement with model predictions. In addition, the experiment result shows that WEAs are present in the sample with 12.9×10^6 RCF cycles under 4.5 GPa, which matches the model prediction that WEA presents after 1.5×10^6 under 4.5 GPa contact stress.
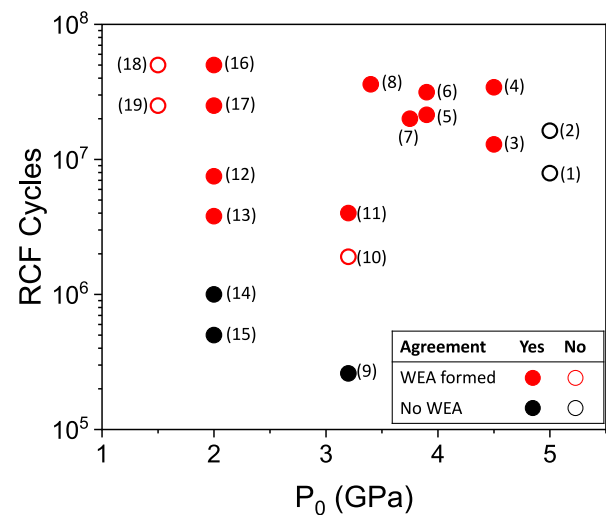
Fig. 5. Literature data and corresponding model result. The numbers displayed next to data points are the experiment numbers shown in Table 4.

3.2. Modelling

The model incorporates many parameters including hydrogen content, maximum contact stress, temperature, rotational speed and others. Therefore, some of the RCF experimental results reported in the literature were selected to further validate the model under different test conditions [6,18–20]. Table 4 summarises those experimental parameters, and the corresponding calculated modelling results are added for comparison. Fig. 5 shows a RCF cycles/P_0 diagram in which the data points showed in Table 4 are plotted. It is worth noting that a L_{10} continuous line is not possible to be added here as the data points are obtained from multiple test geometries with different parameters for L_{10} calculation. It can be seen that the model has a good agreement for most of the cases (~74%). However, there are a few cases that the model has failed to predict the WEA formation, which is discussed in the following section.

4. Discussion

4.1. Dislocation mobility altered by hydrogen

It has been broadly reported that hydrogen can facilitate premature failure in what is known as hydrogen embrittlement. Several mechanisms have been established to account for this phenomenon such as

Table 4
Literature data and corresponding model result.

Exp.	Ref.	Testing method	P_0 (GPa)	$\dot{N}$ (rpm)	T (°C)	H (ppm)	RCF cycles	WEA presence Observation	WEA presence Prediction (Critical cycles)	Agreement
1	This study	Ball-on-rod	5.0	3600	30	5.0	7.9×10^6	N	Y (0.7×10^6)	N
2	This study	Ball-on-rod	5.0	3600	30	5.0	16.3×10^6	N	Y (0.7×10^6)	N
3	This study	Ball-on-rod	4.5	3600	30	5.0	12.9×10^6	Y	Y (1.3×10^6)	Y
4	This study	Ball-on-rod	4.5	3600	30	5.0	34.2×10^6	Y	Y (1.3×10^6)	Y
5	This study	Ball-on-rod	3.9	3600	30	5.0	21.4×10^6	Y	Y (3.6×10^6)	Y
6	This study	Ball-on-rod	3.9	3600	30	5.0	31.4×10^6	Y	Y (3.6×10^6)	Y
7	[20]	Ball-on-rod	3.75	3600	40	5.0	20×10^6	Y	Y (4.9×10^6)	Y
8	[18]	Ball bearing	3.4	2250	25	2.0	36×10^6	Y	Y (21×10^6)	Y
9	[19]	Ball bearing	3.2	6000	83	5.96	0.26×10^6	N	N (2.5×10^6)	Y
10	[19]	Ball bearing	3.2	6000	83	4.30	1.9×10^6	Y	N (2.3×10^6)	N
11	[19]	Ball bearing	3.2	6000	83	4.72	4.0×10^6	Y	Y (2.3×10^6)	Y
12	[6]	Two-roller	2.0	4000	67	1.8	7.5×10^6	Y	Y (2.0×10^6)	Y
13	[6]	Two-roller	2.0	2000	67	1.8	3.8×10^6	Y	Y (1.3×10^6)	Y
14	[6]	Two-roller	2.0	4000	67	1.8	1.0×10^6	N	N (2.0×10^6)	Y
15	[6]	Two-roller	2.0	2000	67	1.8	0.5×10^6	N	N (1.3×10^6)	Y
16	[6]	Two-roller	2.0	4000	67	0.27	50×10^6	Y	Y (7.5×10^6)	Y
17	[6]	Two-roller	2.0	2000	67	0.27	25×10^6	Y	Y (4.8×10^6)	Y
18	[6]	Two-roller	1.5	4000	67	1.8	50×10^6	Y	N (1500×10^6)	N
19	[6]	Two-roller	1.5	2000	67	1.8	25×10^6	Y	N (740×10^6)	N

hydrogen-enhanced decohesion and hydrogen-enhanced local plasticity. These mechanisms interpret hydrogen embrittlement in terms of the interaction between hydrogen and the microstructure, including crystallographic defects. In this study, WEA formation is modelled based on a dislocation-assisted carbon migration theory which assumes carbon atoms can be transported by dislocation glide. The presence of hydrogen does not lead to failure directly; instead, hydrogen modifies the dislocation mobility and further facilitates the carbon migration, which result in the faster formation of WEAs under rolling contact fatigue.

Dislocation mobility can be greatly affected by hydrogen [13,25, 26]. Wang et al. [26] reported the relation between dislocation mobility and hydrogen content by performing a macroscopic stress relaxation experiment. Their relation follows:

$$\frac{V_H}{V_0} = \exp\frac{-\delta\Delta G}{kT}, \tag{9}$$

where $\delta\Delta G$ is the Gibbs free energy. It is worth noting that using the values obtained in their report, the greatest value of $\frac{V_H}{V_0}$ is about 3 which is lower than the value we used in this study. The hydrogen-facilitated WEAs formation should be based on nanoscale hydrogen-dislocation interaction, however the dislocation mobility obtained from macroscopic stress relaxation can be affected by many factors such as forest dislocation density, precipitates, H-vacancy locks and others. The underlying mechanism for WEA formation is the formation of carbon-rich cells which are about 25 nm in diameter. At such scale, the effect from aforementioned factors could be neglected. Therefore, kMC modelling is a suitable technique to model hydrogen-dislocation interactions at the nanoscale.

4.2. Plastic strain accumulation under rolling contact fatigue

For the test performed at $P_0 = 5.0$ GPa in this study, the model overpredicts the formation of WEAs, i.e. the model predicts WEAs should appear with 0.7×10^6 RCF cycles but no WEA is observed in samples with 7.9×10^6 (Exp. 1 in Table 4) and 16.3×10^6 (Exp. 2 in Table 4) RCF cycles. This is due to excessive microplasticity with higher applied stress. Kang et al. [28] have investigated the subsurface hardening with different maximum contact pressures. Their results demonstrated that, with 10^7 RCF cycles, an increase in hardness in the sample subsurface of ~ 20 H_V was obtained with $P_0 = 3.7$ GPa whilst an increase of ~ 80 H_V with $P_0 = 5.6$ GPa. This implies that significant subsurface plastic deformation can be introduced with high contact stresses, leading to an alteration of subsurface dislocation kinetics. On the other hand, the model shows an underestimation for $P_0 < 2.0$ GPa (Exp. 18 and

Exp. 19 in Table 4). This may be due to insufficient stress to trigger dislocation activity. It follows that the model of strain accumulation under RCF needs improvement to accommodate for a wider range of contact stresses.

4.3. Links between WEA formation and RCF life

It has been suggested that WEAs in bearing components appear usually around $0.001L_{10}$ [1]. A plot of L_{10} is added in Fig. 4(a) to compare with the modelled WEA formation lines. The L_{10} line lays precisely between the no hydrogen (0 ppm) line and the 0.27 ppm hydrogen lines. L_{10} slope approaches that of WEA formation in the RCF life cycles/P_0 diagram; this result suggests that industrial bearings life may be affected by even small hydrogen contents, with RCF life variation with contact pressure being masked by statistical variations. In addition, the bearing life could be shortened with the presence of WEAs resulting from other defects. Liang et al. [21] reported that hydrogen may facilitate the formation of voids and microcracks in bearings. Such defects could lead to crack development in bearings, resulting in premature failure together with WEAs formation. Further development in RCF life estimation is necessary for bearing components with hydrogen.

4.4. Implications for steel production

Fig. 4(a) reveals that even small traces of hydrogen can significantly reduce bearing life. A content of 0.27 ppm of hydrogen accelerates WEA formation ~ 5 times, whereas 1.8 ppm accelerates ~ 30 times. Typically, steel production restricts hydrogen to a maximum of 1 ppm for bearing applications. The result shown here imply that hydrogen already plays a significant role in WEA formation, and thus life, at well-accepted bearing hydrogen contents. It follows that a possible factor adding to the scatter in bearing life prediction is hydrogen, even if present in the steel rod and in the absence of environmental effects. Calculations show that 1 ppm hydrogen accelerates WEA formation by an order of magnitude, proportionally reducing bearing life.

5. Conclusion

In summary, by correcting the expression for dislocation-assisted carbon flux in the presence of hydrogen, the proposed model is able to predict the early formation of white etching areas under rolling contact fatigue. This model incorporates the amount of hydrogen, maximum contact stress, temperature, rotational speed and other factors. This approach provides a quantitative tool to predict bearing life when

hydrogen is present. Further model improvement is needed to accommodate very high (> 4.5 GPa) and very low (< 2.0 GPa) contact pressures.

Declaration of competing interest

The authors declare that they have no known competing financial interests or personal relationships that could have appeared to influence the work reported in this paper.

Acknowledgements

References

[1] Bhadeshia HKDH. Steels for bearings. Prog Mater Sci 2012;57(2):268–435.

[2] Fu H, Galindo-Nava EI, Rivera-Díaz-del-Castillo PEJ. Modelling and characterisation of stress-induced carbide precipitation in bearing steels under rolling contact fatigue. Acta Mater 2017;128:176–87.

[3] Fu H, Song W, Galindo-Nava EI, Rivera-Díaz-del-Castillo PEJ. Strain-induced martensite decay in bearing steels under rolling contact fatigue: Modelling and atomic-scale characterisation. Acta Mater 2017;139:163–73.

[4] Fu H, Rivera-Díaz-del Castillo PEJ. A unified theory for microstructural alterations in bearing steels under rolling contact fatigue. Acta Mater 2018;155:43–55.

[5] Fu H, Rydel JJ, Gola AM, Yu F, Geng K, Lau C, et al. The relationship between 100Cr6 steelmaking, inclusion microstructure and rolling contact fatigue performance. Int J Fatigue 2018.

[6] Evans MH, Richardson AD, Wang L, Wood RJK. Effect of hydrogen on butterfly and white etching crack (WEC) formation under rolling contact fatigue (RCF). Wear 2013;306(1):226–41.

[7] Curd ME, Burnett TL, Fellowes J, Donoghue J, Yan P, Withers PJ. The heterogenous distribution of white etching matter (WEM) around subsurface cracks in bearing steels. Acta Mater 2019;174:300–9.

[8] Curd ME, Burnett TL, Fellowes J, Yan P, Withers PJ. Redistribution of carbon caused by butterfly defects in bearing steels. Acta Mater 2020;183:390–7.

[9] Mayweg D, Morsdorf L, Li Y, Herbig M. Correlation between grain size and carbon content in white etching areas in bearings. Acta Mater 2021;117048.

[10] Evans MH, Walker JC, Ma C, Wang L, Wood RJK. A FIB/TEM study of butterfly crack formation and white etching area (WEA) microstructural changes under rolling contact fatigue in 100Cr6 bearing steel. Mater Sci Eng A 2013;570:127–34.

[11] Grabulov A, Ziese U, Zandbergen HW. TEM/SEM investigation of microstructural changes within the white etching area under rolling contact fatigue and 3-D crack reconstruction by focused ion beam. Scr Mater 2007;57(7):635–8.

[12] Kürten D, Khader I, Raga R, Casajús P, Winzer N, Kailer A, et al. Hydrogen assisted rolling contact fatigue due to lubricant degradation and formation of white etching areas. Eng Fail Anal 2019;99:330–42.

[13] Katzarov IH, Pashov DL, Paxton AT. Hydrogen embrittlement I. Analysis of hydrogen-enhanced localized plasticity: Effect of hydrogen on the velocity of screw dislocations in α-Fe. Phys Rev Mater 2017;1(3):033602.

[14] Stopher MA, Rivera-Díaz-del-Castillo PEJ. Hydrogen embrittlement in bearing steels. Mater Sci Technol 2016;32(11):1184–93.

[15] Bhadeshia HKDH. Prevention of hydrogen embrittlement in steels. ISIJ Int 2016;56(1):24–36.

[16] Liang XZ, Zhao GH, Dodge MF, Lee TL, Dong HB, Rivera-Díaz-del Castillo PEJ. Hydrogen embrittlement in super duplex stainless steels. Materialia 2020;9:100524.

[17] Kino N, Otani K. The influence of hydrogen on rolling contact fatigue life and its improvement. JSAE Rev 2003;24(3):289–94.

[18] Ruellan A, Ville F, Kleber X, Arnaudon A, Girodin D. Understanding white etching cracks in rolling element bearings: The effect of hydrogen charging on the formation mechanisms. Proc Inst Mech Eng J 2014;228(11):1252–65.

[19] Vegter RH, Slycke JT. The role of hydrogen on rolling contact fatigue response of rolling element bearings. J ASTM Int 2009;7(2):1–12.

[20] Szost BA, Rivera-Díaz-del-Castillo PEJ. Unveiling the nature of hydrogen embrittlement in bearing steels employing a new technique. Scr Mater 2013;68(7):467–70.

[21] Liang XZ, Zhao G-H, Owens J, Gong P, Rainforth WM, Rivera-Díaz-del Castillo PEJ. Hydrogen-assisted microcrack formation in bearing steels under rolling contact fatigue. Int J Fatigue 2020;134:105485.

[22] Winzer N, Khader I. Hydrogen diffusion and trapping in bodies undergoing rolling contact. Wear 2013;303(1–2):451–8.

[23] Khader I, Kürten D, Raga R, Winzer N, Kailer A. Modeling hydrogen diffusion in a tribological scenario: A failure analysis of a thrust bearing. Wear 2019;438:203054.

[24] Kürten D, Khader I, Kailer A. Determining the effective hydrogen diffusion coefficient in 100Cr6. Mater Corros 2020;71(6):918–23.

[25] Wang S, Hashimoto N, Ohnuki S. Effects of hydrogen on activation volume and density of mobile dislocations in iron-based alloy. Mater Sci Eng A 2013;562:101–8.

[26] Wang S, Hashimoto N, Wang Y, Ohnuki S. Activation volume and density of mobile dislocations in hydrogen-charged iron. Acta Mater 2013;61(13):4734–42.

[27] Kang J-H, Hosseinkhani B, Williams CA, Moody MP, Bagot PAJ, Rivera-Díaz-del Castillo PEJ. Solute redistribution in the nanocrystalline structure formed in bearing steels. Scr Mater 2013;69(8):630–3.

[28] Kang J-H, Vegter RH, Rivera-Díaz-del Castillo PEJ. Rolling contact fatigue in martensitic 100Cr6: Subsurface hardening and crack formation. Mater Sci Eng A 2014;607:328–33.

[29] Kang J-H, Rivera-Díaz-del Castillo PEJ. Fatigue in martensitic 100Cr6: Relationship between rolling contact fatigue microstructural transitions and repetitive push testing. Mater Sci Eng A 2014;614:214–22.

[30] Pavlina EJ, Van Tyne CJ. Correlation of yield strength and tensile strength with hardness for steels. J Mater Eng Perform 2008;17(6):888–93.

[31] Liang XZ, Dodge MF, Dong HB. Using transmission kikuchi diffraction in a scanning electron microscope to quantify geometrically necessary dislocation density at the nanoscale. Ultramicroscopy 2019;197:39–45.

[32] Cottrell AH, Bilby BA. Dislocation theory of yielding and strain ageing of iron. Proc Phys Soc 1949;62(1):49.

[33] Kang J-H, Hosseinkhani B, Vegter RH, Rivera-Díaz-del Castillo PEJ. Modelling dislocation assisted tempering during rolling contact fatigue in bearing steels. Int J Fatigue 2015;75:115–25.

[34] Bhadeshia H, Honeycombe R. Steels microstructure and properties. Oxford: Elsevier; 2006.